methods

Label-free quantitative analysis of lipid metabolism in living *Caenorhabditis elegans*

Thuc T. Le,* Holli M. Duren,† Mikhail N. Slipchenko,* Chang-Deng Hu,[1,†,§] and Ji-Xin Cheng[1,*,§,]**

Weldon School of Biomedical Engineering,* Department of Medicinal Chemistry and Molecular Pharmacology,† Purdue Cancer Center,§ and Department of Chemistry,** Purdue University, West Lafayette, IN 47907

Abstract The ubiquity of lipids in biological structures and functions suggests that lipid metabolisms are highly regulated. However, current invasive techniques for lipid studies prevent characterization of the dynamic interactions between various lipid metabolism pathways. Here, we describe a noninvasive approach to study lipid metabolisms using a multifunctional coherent anti-Stokes Raman scattering (CARS) microscope. Using living *Caenorhabditis elegans* as a model organism, we report label-free visualization of coexisting neutral and autofluorescent lipid species. We find that the relative expression level of neutral and autofluorescent lipid species can be used to assay the genotype-phenotype relationship of mutant *C. elegans* with deletions in the genes encoding lipid synthesis transcription factors, LDL receptors, transforming growth factor β receptors, lipid desaturation enzymes, and antioxidant enzymes. Furthermore, by coupling CARS with fingerprint confocal Raman analysis, we analyze the unsaturation level of lipids in wild-type and mutant *C. elegans*. Our study shows that complex genotype-phenotype relationships between lipid storage, peroxidation, and desaturation can be rapidly and quantitatively analyzed in a single living *C. elegans*.—Le, T. T., H. M. Duren, M. N. Slipchenko, C-D. Hu, and J-X. Cheng. **Label-free quantitative analysis of lipid metabolism in living Caenorhabditis elegans. *J. Lipid Res.* 2010.** 51: **672–677.**

Supplementary key words cholesterol synthesis • coherent anti-Stokes Raman scattering • lipid desaturation • label-free imaging • lipid storage • peroxidation • spontaneous Raman spectroscopy • two-photon excited fluorescence

With short lifespan, rapid reproduction cycle, amenable genetics, and a remarkable conservation of human disease genes and pathways, *Caenorhabditis elegans* has become an ideal model to study the mechanisms of disease pathogenesis (1). Being optically transparent, *C. elegans* has been extensively employed to visualize lipid storage with fluorescent imaging of lipids stained with Nile Red (2, 3) or recently with label-free single-frequency coherent anti-Stokes Raman scattering (CARS) imaging (4). However, either fluorescent or single-frequency CARS imaging lacks spectral information critical for lipid composition analysis. Although spontaneous Raman microscopy (5) and multiplex CARS microscopy (6) could analyze the composition of single lipid droplets, their image acquisition speeds are too slow for live-cell or animal study. Alternatively, third harmonic generation microscopy can visualize lipid droplets using optical heterogeneity of biological samples for contrast mechanism (7). However, third harmonic generation lacks chemical selectivity to analyze lipid composition. Consequently, a microscopy tool to study critical aspects of lipid metabolism, including lipid storage and composition, is lacking. By employing a multifunctional microscope that permits high-speed CARS imaging, two-photon excited fluorescence (TPEF) imaging, and confocal Raman spectral analysis with a picosecond laser source (8, 9), we demonstrate the capability to study the dynamic interactions between lipid storage, peroxidation, and desaturation in wild-type and mutant *C. elegans*.

This work is supported by a National Institutes of Health postdoctoral fellowship (F32HL089074 to T.T.L.), National Institutes of Health Grant R01EB007243 (to J-X.C.), and National Science Foundation Grant MCB0420634 (to C-D.H.). Its contents are solely the responsibility of the authors and do not necessarily represent the official views of the National Institutes of Health. T.T. L. and H.M.D. designed and performed experiments. T.T.L. and M.N.S. analyzed data. J-X.C. and C-D.H. contributed analytical tools, reagents, and research guidance. T.T.L and H.M.D wrote the article. All authors read and approved the final manuscript.

Manuscript received 31 July 2009 and in revised form 29 September 2009.

Published, JLR Papers in Press, September 29, 2009
DOI 10.1194/jlr.D000638

Abbreviations: CARS, coherent anti-Stokes Raman scattering; RME-2, receptor-mediated endocytosis 2; SREBP-1, sterol regulatory element binding protein 1; TPEF, two-photon excited fluorescence.

[1]To whom correspondence should be addressed.
e-mail: cdhu@pharmacy.purdue.edu (C-D.H.); jcheng@purdue.edu (J-X.C.)

The online version of this article (available at http://www.jlr.org) contains supplementary data in the form of three figures and one video.

METHODS

A multifunctional CARS microscope

A spectrometer with a 300 g/mm grating and a thermoelectrically cooled back-illuminated EMCCD (Newton 920-BRD; Andor Technology, Belfast, Ireland) is mounted to the side port of a laser scanning microscope (IX71/FV300; Olympus, Center Valley, PA) to allow TPEF imaging, CARS imaging, and spontaneous Raman spectral analysis on the same platform. Pump and Stokes lasers are tuned to 14,140 cm^{-1} and 11,300 cm^{-1}, respectively, to be in resonance with the CH_2 symmetric stretch vibration at 2,840 cm^{-1}. The combined beams are focused into the sample through a ×60 water immersion microscope objective with a 1.2 numerical aperture. Forward-detected CARS signal is collected by an air condenser with a 0.55 numerical aperture, transmitted through a 600/65 nm band-pass filter, and detected by a photomultiplier tube (H7422-40; Hamamatsu, Japan). Simultaneously, back-reflected TPEF signal is collected by the same illuminating objective, spectrally separated from the excitation source, transmitted through a 520/40 nm band-pass filter, and detected by a photomultiplier tube (H7422-40; Hamamatsu) mounted at the back port of the microscope. Following CARS and TPEF imaging, the Stokes beam is blocked and the pump laser-induced Raman scattering signal is directed toward the spectrometer to permit spectral analysis from 830 to 3,100 cm^{-1}, which covers both the fingerprint and the CH-stretch vibration regions. Due to the utilization of a confocal pinhole with a diameter of 50 μm before the spectrometer, the Raman signals arise from a focal volume of 2.3 femtoliter at the center of the field of view of a CARS image. Average acquisition time for a 512 × 512 pixel CARS image is 1.12 s, and a full-spectral Raman analysis is 4 s. The combined Stokes and pump laser power is kept constantly at 40 mW. For all Raman spectral measurements, pump laser power is reduced to 10 mW. Variability in Raman spectral measurements of neutral lipid droplets is discussed in supplementary Figs. II and III. Experimental details of Rama spectra acquisition and data analysis were previously described by Slipchenko et al. (9).

Imaging conditions and data analysis

All *C. elegans* were anesthetized in a droplet of 100 mM sodium azide and mounted on fresh 2% agarose slides prior to imaging. To evaluate the expression level of neutral and autofluorescent lipid droplets, we define a probed volume with xyz dimensions of 125 × 125 × 35 μm. We first locate the midsection of an adult wild-type or mutant *C. elegans* and then perform simultaneous depth imaging with CARS and TPEF along the vertical (z) axis at 1 μm step size to obtain 36 frames. Background CARS and TPEF pixel intensity are subtracted from average pixel intensity of CARS and TPEF signals of the probed volume to obtain the expression level of neutral and autofluorescent lipid droplets, respectively. Background CARS and TPEF pixel intensity are defined as the average pixel intensity of probed volumes devoid of neutral and autofluorescent lipid droplets. The background CARS signal includes signals arising from the worm bodies. The expression levels of neutral and autofluorescent lipid droplets are adjusted to 1 for the wild type and comparatively for mutant *C. elegans*. Because CARS signal is quadratically dependent on the concentration of CH_2 molecular vibration at $\omega_p - \omega_S = 2{,}840\ cm^{-1}$, we present the square root value of CARS signal as the expression level of neutral lipid droplets.

C. elegans strains

All *C. elegans* strains were obtained from the *Caenorhabditis* Genetics Center: wild-type Bristol (N2), BX107 [*fat-5(tm420)*], BX106 [*fat-6(tm331)*], BX153 [*fat-7(wa36)*], BX160 [*fat-5(tm420)/fat-6(tm331)*], BX156 [*fat-6(tm331)/fat-7(wa36)*], BX110 [*fat-5(tm420)/fat-7(wa36)*], CE833 [*sbp-1(ep176)*], FX776 [*sod-1(tm776)*], CB1364 [*daf-4(e1364)*], and DH1390 [*rme-2(b1008)*]. Except for CE833 [*sbp-1(ep176)*], which was cultured at 15°C, all *C. elegans* strains were cultured on agar plates seeded with OP50 *Escherichia coli* at 20°C.

Biochemical assays

Experimental details of gas chromatography and mass spectrometry analysis of fatty acids composition have been previously described (10). Cholesterol, phosphatidylcholine, and superoxide dismutase were performed using commercially available kits according to manufacturer's protocols (catalog numbers 10007640, 10009926, and 706002; Cayman Chemical, Ann Arbor, MI). To collect worms, 16 cm plates were washed with M9 media into Eppendorf tubes. Worms were further washed multiple times with M9 media to remove any residual bacteria. The expression level of phosphatidylcholine was used as a reference to adjust for the number of *C. elegans* analyzed.

RESULTS

By simultaneous CARS and TPEF imaging of living *C. elegans*, we discovered two distinctive lipid species (**Fig. 1**; see supplementary Video I). One lipid species can be visualized by CARS only, which we identify as neutral lipid (Fig. 1A). Visualization of such neutral lipid species with CARS has been previously reported by Hellerer et al. (4). The other lipid species can be visualized by both autofluorescent signals identifiable with TPEF imaging and lipid signals identifiable with CARS imaging (Fig. 1B, C). Further confocal Raman spectral analyses of the neutral lipid droplets reveal strong chemical signatures typical of tria-

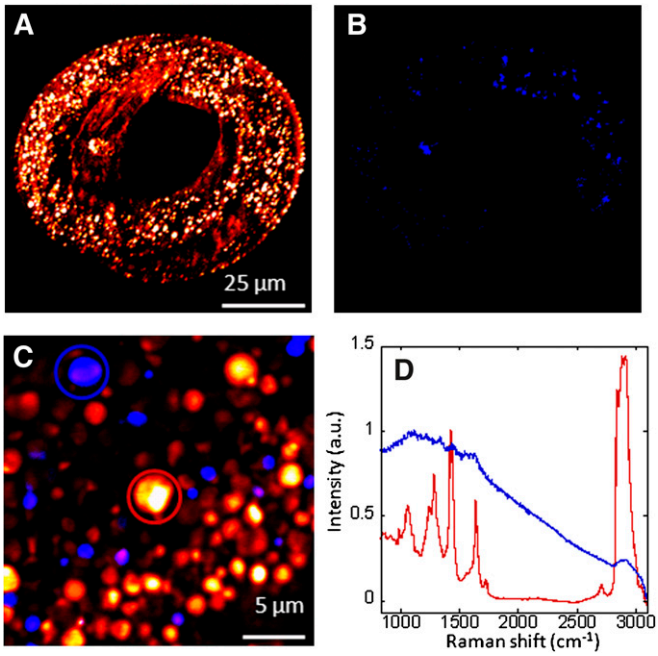

Fig. 1. Chemical imaging and spectral analysis of lipid species in *C. elegans*. CARS (A; red) and TPEF (B; blue) imaging of a larval L2 *C. elegans*. Images presented as a three-dimensional projection of 25 frames taken along vertical axis at 1 μm intervals. C: An enlarged and overlaid image of lipid species in *C. elegans*. D: Spontaneous Raman spectral analysis of neutral lipid droplets (red) and autofluorescent lipid droplets (blue).

cylglycerides (Fig. 1D). In contrast, the fluorescence from the autofluorescent lipid droplets dominates the Raman spectra (Fig. 1D). Several previous studies have also identified such autofluorescent particles and associated them with lipids, oxidative stress, and lifespan of *C. elegans* (11, 12).

To explore the potential of using the neutral and autofluorescent lipid species as a readout of lipid metabolism, we evaluated their expression levels in wild-type and mutant *C. elegans*. All selected *C. elegans* mutants have been well characterized, with deletions in the genes encoding lipid metabolism proteins, including Δ9 desaturases (palmitoyl-CoA desaturase *fat-5* and stearoyl-CoA desaturases *fat-6* and *fat-7*) (10), sterol regulatory element binding protein (*sbp-1*) (13, 14), copper/zinc superoxide dismutase (*sod-1*) (15, 16), type II transforming growth factor β receptor (*daf-4*) (4, 17), and LDL receptor (*rme-2*)18. Specifically, Δ9 desaturases are lipogenic enzymes critical for the conversion of saturated fatty acids into monounsaturated fatty acids (19, 20). Sterol regulatory element binding protein 1 (SREBP-1) is a transcription factor that controls the expression of lipogenic enzymes (14). Superoxide dismutase is an antioxidant enzyme that protects cells from reactive oxygen species (15). Type II transforming growth factor β receptor is a transmembrane serine/threonine kinase whose functions are implicated in many biological processes, including the insulin signaling pathway (17). Receptor-mediated endocytosis 2 (RME-2) is an LDL receptor that mediates yolk endocytosis and fatty acid transport in oocytes (18). Although the functions of these lipid metabolism proteins are well understood, their roles in the expression level of autofluorescent lipid species in *C. elegans* have not been characterized.

Our analyses of neutral and autofluorescent lipid droplet expression level in *C. elegans* mutants reveal five distinctive phenotypes as compared to the wild type (**Fig. 2A**). The first phenotype is observed in *C. elegans* mutants with double deletion of Δ9 desaturases, *fat-5/fat-6*, where a 1.4-fold decrease in the expression level of neutral lipid droplets is accompanied by a 3-fold increase in the expression level of autofluorescent lipid droplets (Fig. 2A–C). This phenotype is consistent with previous biochemical analyses where a decrease in fat storage and an increase in the expression of genes involved in fatty acid oxidation are observed in Δ9 desaturase mutants (10). The second phenotype is observed in *sbp-1* mutants, where there is a near complete suppression of both neutral and autofluorescent lipid droplet expression (Fig. 2A–C). This phenotype is also supported by the established roles of SREBP-1 in cholesterol and fatty acids homeostasis (14). The third phenotype is observed with *sod-1* mutants, where the wild-type level of neutral lipid droplet expression is accompanied by a 2-fold increase in autofluorescent lipid droplet expression (Fig. 2A–C). This phenotype suggests a direct role of antioxidant enzymes in regulating the level of autofluorescent lipid droplets. The fourth phenotype is observed with *daf-4* mutants, where a 1.4-fold increase in neutral lipid droplet is accompanied by a 2-fold reduction in autofluorescent lipid droplet compared to the wild type (Fig. 2A–C). This increase in neutral lipid storage in *daf-4* mutants has also been reported by Hellerer et al. (4). However, the effect of *daf-4* deletion on the decrease of autofluorescent lipid droplet level is reported here for the first time. Finally, the fifth phenotype is observed with *rme-2* mutants, where a 1.3-fold increase in the expression of neutral lipid droplets is accompanied by a wild-type level expression of autofluorescent lipid droplets (Fig. 2A–C). This phenotype suggests a possible role of RME-2 in neutral lipid droplet formation. However, this relationship has not been elucidated in the current literature. Taken together, our results show that the relative expression levels of neutral and autofluorescent lipid species provide a reliable means to assay for phenotypes of *C. elegans* mutants.

Using biochemical assays, we find that changes in the level of autofluorescent lipid species in *fat-5/fat-6*, *sbp-1*, and *sod-1* mutants are due to distinct mechanisms (Fig. 2D). By measuring the cholesterol level in total lipid extracts, we find a 1.2-fold increase in *fat-5/fat-6* mutants, a 4-fold reduction in *sbp-1* mutants, and no change in *sod-1* mutants. These observations suggest that Δ9 desaturases and SREBP-1 are involved in cholesterol biosynthesis, whereas superoxide dismutase is not. Therefore, increases in autofluorescent lipid species observed in *fat-5/fat-6* and *sbp-1* mutants are likely due to a different mechanism compared to *sod-1* mutants (Fig. 2D).

By CARS imaging and spontaneous Raman analysis of single lipid droplets, we further evaluated the degree of lipid-chain unsaturation in wide-type and mutant *C. elegans*. Using C18 fatty acid methyl esters as standards, we show that the degree of lipid-chain unsaturation can be measured using three Raman-active bands, including 1280 cm^{-1}, 1660 cm^{-1}, and 3015 cm^{-1} (**Fig. 3A–C**) (6, 21). Because the signal-to-noise ratio for C=C stretch is highest at 1660 cm^{-1} band, we select this band to evaluate lipid chain unsaturation (6). We observe that I_{1660}/I_{1445} is linearly correlated with lipid chain unsaturation (Fig. 3C). Using I_{1660}/I_{1445} as a reliable measure of Δ9 desaturase enzymatic activity, we systematically evaluated lipid chain unsaturation of neutral lipid droplets. We observed significant reduction in C=C stretch vibration signal in Δ9 desaturase mutants compared to wild-type *C. elegans* (Fig. 3D). Quantitative analysis of lipid droplet I_{1660}/I_{1445} in six desaturase mutants reveals up to 2-fold reduction in lipid chain unsaturation in single and double Δ9 desaturase mutants (Fig. 3E). Our Raman spectral analyses are further supported by GC-MS measurements of lipid chain unsaturation of total lipid extracts (see supplementary Fig. I). We find a dramatic decrease in the ratios of unsaturated oleic, linoleic, and eicosenoic fatty acids over saturated stearic acid in *fat-5/fat-6* and *fat-6/fat-7* mutants compared to the wild type (Fig. 3F). Complete analyses of lipid composition of Δ9 desaturase mutants using GC-MS have been described previously (10). However, unlike GC-MS, the combination of CARS imaging and confocal Raman spectral analysis, so called compound Raman microscopy (6), enabled us to measure lipid chain desaturation noninvasively with single lipid droplet sensitivity. This capability should allow real-time dynamic studies of the activity of desaturases and other lipid metabolism enzymes in living *C. elegans*.

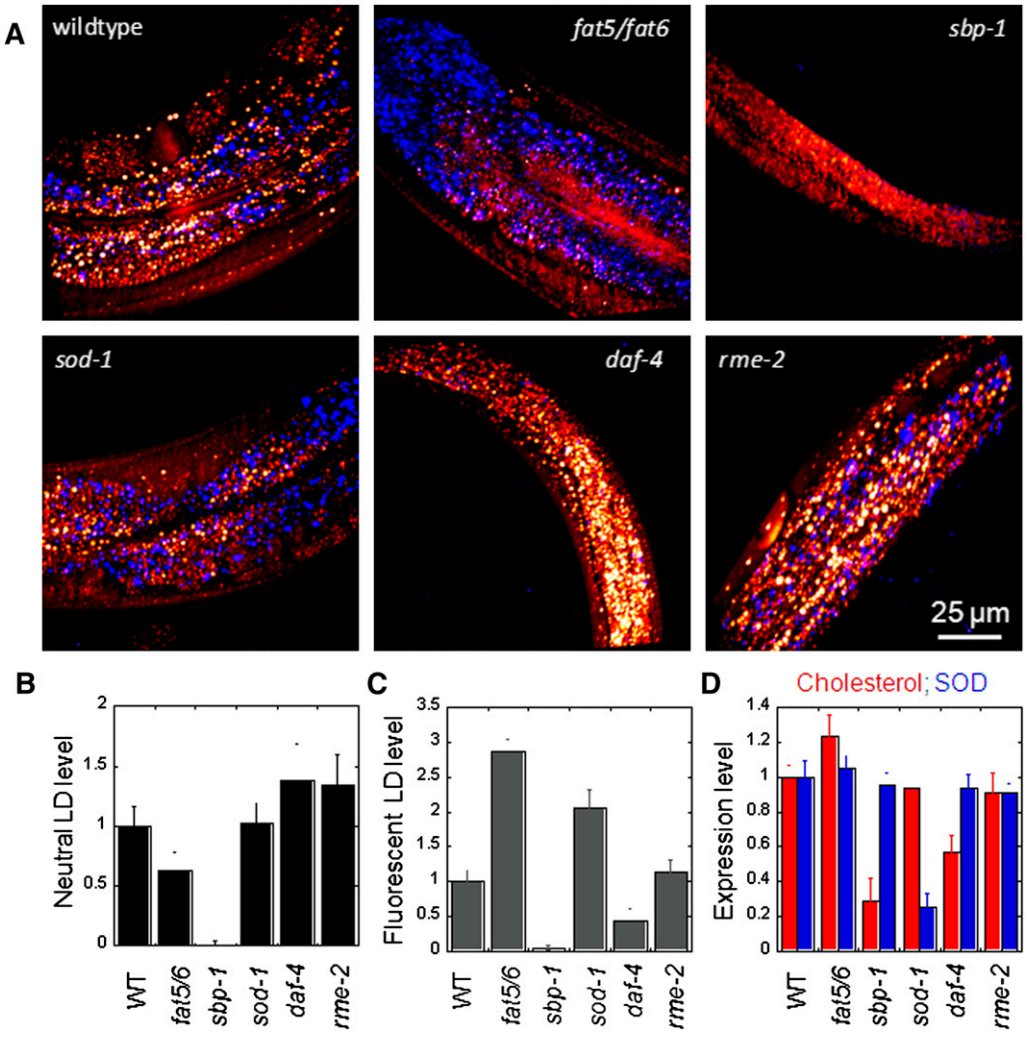

Fig. 2. Expression levels of lipid species in the wild type and mutant *C. elegans*. A: CARS imaging of lipid (red) and TPEF imaging of autofluorescent lipid species (blue) of adult N2 wild-type and mutant *C. elegans*. Images are presented as three-dimensional projections of 36 frames taken along the vertical axis at 1 μm intervals. Expression levels of neutral lipid droplets (B) and autofluorescent lipid droplets (C) as a function of wild-type and mutant worms. Expression levels are normalized to 1 for the wild type and comparatively for mutants. Error bars represent distribution six adult wild-type or mutant *C. elegans*. D: Biochemical measurements of cholesterol level and superoxide dismutase (SOD) activity. Expression levels are normalized to 1 for the wild type and comparatively for mutant *C. elegans*. Error bars represent distribution across three repeated experiments.

DISCUSSION

In this study, we report label-free visualization and quantitation of coexisting neutral and autofluorescent lipid species in living *C. elegans*. We show that multimodal imaging allows rapid genotype-phenotype screening of lipid metabolism in *C. elegans*. Specifically, we find that the expression of neutral and autofluorescent lipid species are dynamically correlated to specific genes. Deletion of SREBP-1 transcription factor for lipid and cholesterol synthesis suppresses both neutral and autofluorescent lipid droplet formation. Deletion of Δ9 desaturases represses neutral lipid-droplet formation and promotes autofluorescent lipid droplet formation. Conversely, deletion of transforming growth factor β receptor represses autofluorescent lipid droplet formation and promotes neutral autofluorescent lipid droplet formation. These observations suggest that SREBP-1, Δ9 desaturases, and transforming growth factor β receptor participate in shared pathways by both neutral and autofluorescent lipid droplet formation. In contrast, deletion of antioxidant enzymes affects only autofluorescent lipid droplet formation, and deletion of LDL receptor RME-2 affects only neutral lipid droplet formation. These observations suggest that antioxidant enzymes or LDL receptor RME-2 participates in specific autofluorescent or neutral lipid droplet formation pathways, respectively. Thus, the relationship between the expression levels of neutral and autofluorescent lipid species could potentially be used to identify the involvement of unknown proteins in lipid metabolism pathways.

In addition to visualization of neutral and autofluorescent lipid species with CARS and TPEF signals, spontaneous

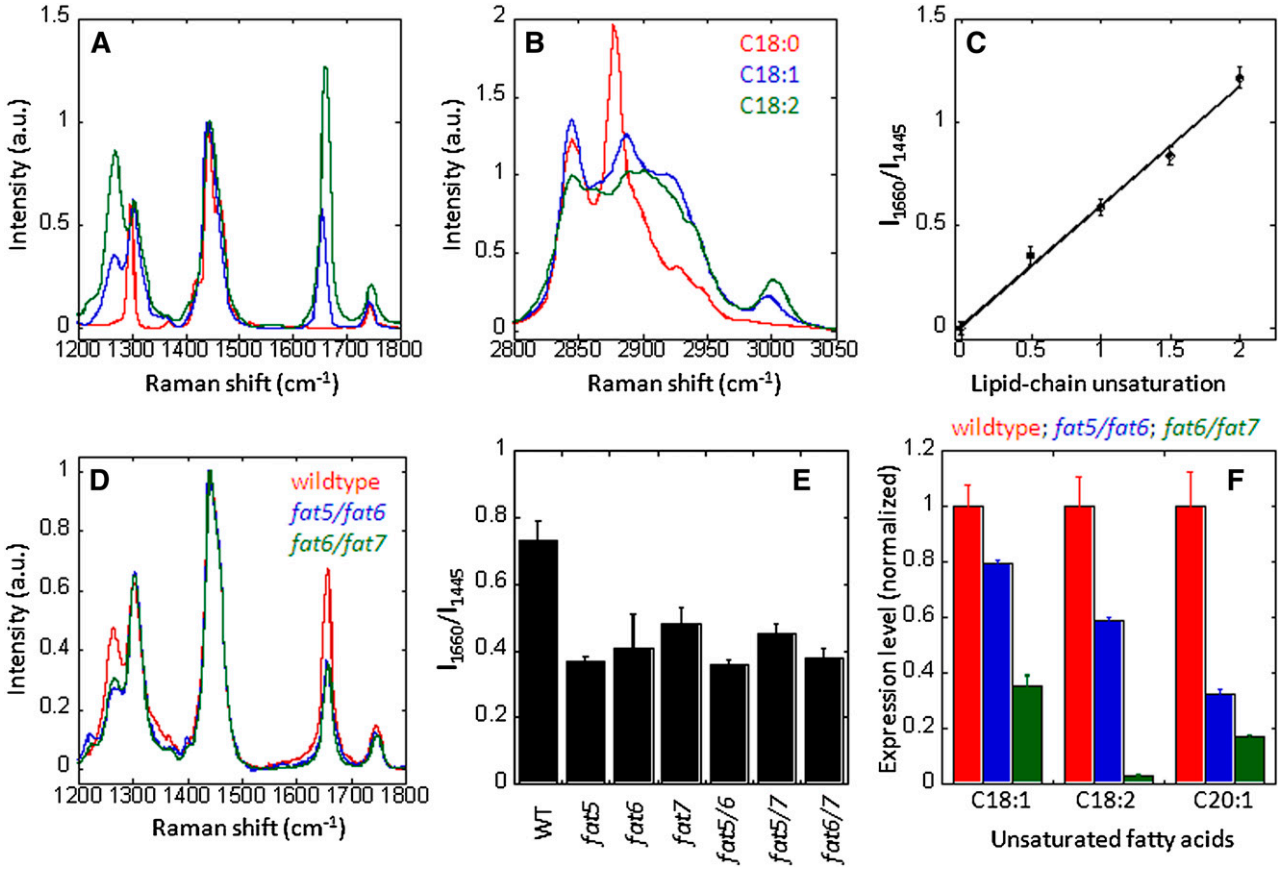

Fig. 3. Analysis of lipid chain unsaturation in Δ9 desaturase wild-type and mutant *C. elegans*. Raman spectra of fatty acid methyl esters: stearate (C18:0), oleate (C18:1), and linoleate (C18:2) at fingerprint region from 1,200 to 1,800 cm^{-1} (A) and the CH-stretch vibration region from 2,800 to 3,100 cm^{-1} (B). C: I_{1660}/I_{1445} as a function of lipid chain unsaturation of stearate, stearate:oleate 1-to-1 mixture, oleate, oleate:linoleate 1-to-1 mixture, and linoleate. Error bars represent distribution across three repeated experiments. D: Representative Raman spectra of neutral lipid droplets in wild-type and mutant *C. elegans*. E: Quantitative analyses of lipid chain unsaturation of lipid droplets in wild-type and Δ9 desaturase mutants. Error bars represent distribution across 18 lipid droplets measured in six adult wild-type or mutant *C. elegans*. F: GC-MS analysis of fatty acids composition of wild-type and Δ9 desaturase double mutants. The ratio of unsaturated fatty acids over C18:0 is normalized to 1 for the wild type and comparatively for mutants. Error bars represent distribution across three repeated experiments.

Raman microspectroscopy enables noninvasive quantitation of desaturation in single lipid droplets. In general, lipid storage, peroxidation, and desaturation are all critical to the health of animals. Indeed, lipid peroxidation is strongly linked to the lifespan of animals (22). Loss of stearoyl-CoA desaturase-1 function has been shown to reduce body adiposity, increase insulin sensitivity, and resistance to diet-induced adiposity in mice (19). However, loss of stearoyl-CoA desaturase-1 function is also associated with increased aorta atherosclerosis (23) and inflammation (24). Nonetheless, the impacts of lipid desaturation on lipid storage, peroxidation, or inflammation are not clearly understood. Herein, we report that genetic deletions of Δ9 desaturase genes in *C. elegans* are strongly associated with a reduction of lipid chain unsaturation (Fig. 3E) and neutral lipid storage (Fig. 2B) as well as a significant increase in autofluorescent lipid species (Fig. 2C) and cholesterol synthesis (Fig. 2D). Given the strong conservation in lipid metabolism from *C. elegans* to humans (1), it is conceivable that future in-depth investigation of lipid desaturation in *C. elegans* could bring new insights to the roles of desaturases in human health and diseases.

Lipids play a ubiquitous role in human physiology. Membrane lipids actively regulate cell proliferation, apoptosis, migration, and senescence (25). Lipid-mediated endocrine networks regulate systemic metabolic homeostasis (26). Excessive lipid storage in obesity is associated with increased risk factors for diabetes, cardiovascular diseases, stroke, and cancer (27). Given the significance of lipids in biology, lipid metabolism should be thoroughly and systematically studied. The multifunctional CARS microscope described in this article, when combined with recent advances in genetics (28) and high-throughput screening (29) for *C. elegans* research, should enable functional studies of lipid metabolism enzymes, interaction of lipid metabolism networks, and discovery of new lipid metabolism pathways. Because CARS microscopy has been applied for in vivo imaging (30–32), our lipid metabolism studies in living *C. elegans* should be extensible to both animals and humans. The versatility of the multifunctional CARS microscope would render it an indispensible tool to the study of lipids in diseases.

The authors thank Han-Wei Wang for help with experiments.

REFERENCES

1. Kaletta, T., and M. O. Hengartner. 2006. Finding function in novel targets: *C. elegans* as a model organism. *Nat. Rev. Drug Discov.* **5:** 387–398.
2. Ashrafi, K., F. Y. Chang, J. L. Watts, A. G. Fraser, R. S. Kamath, J. Ahringer, and G. Ruvkun. 2003. Genome-wide RNAi analysis of *Caenorhabditis elegans* fat regulatory genes. *Nature.* **421:** 268–272.
3. Wang, M. C., E. J. O'Rourke, and G. Ruvkun. 2008. Fat metabolism links germline stem cells and longevity in *C. elegans*. *Science.* **322:** 957–960.
4. Hellerer, T., C. Axang, C. Brackmann, P. Hillertz, M. Pilon, and A. Enejder. 2007. Monitoring of lipid storage in *Caenorhabditis elegans* using coherent anti-Stokes Raman scattering (CARS) microscopy. *Proc. Natl. Acad. Sci. USA.* **104:** 14658–14663.
5. van Manen, H. J., Y. M. Kraan, D. Roos, and C. Otto. 2005. Single-cell Raman and fluorescence microscopy reveal the association of lipid bodies with phagosomes in leukocytes. *Proc. Natl. Acad. Sci. USA.* **102:** 10159–10164.
6. Rinia, H. A., K. N. J. Burger, M. Bonn, and M. Muller. 2008. Quantitative label-free imaging of lipid composition and packing of individual cellular lipid droplets using multiplex CARS microscopy. *Biophys. J.* **95:** 4908–4914.
7. Debarre, D., W. Supatto, A. M. Pena, A. Fabre, T. Tordjmann, L. Combettes, M. C. Schanne-Klein, and E. Beaurepaire. 2006. Imaging lipid bodies in cells and tissues using third-harmonic generation microscopy. *Nat. Methods.* **3:** 47–53.
8. Wang, H. W., T. T. Le, and J. X. Cheng. 2008. Label-free imaging of arterial cells and extracellular matrix using a multimodal CARS microscope. *Opt. Commun.* **281:** 1813–1822.
9. Slipchenko, M. N., T. T. Le, H. Chen, and J. X. Cheng. 2009. High-speed vibrational imaging and spectral analysis of lipid bodies by compound Raman microscopy. *J. Phys. Chem. B.* **113:** 7681–7686.
10. Brock, T. J., J. Browse, and J. L. Watts. 2007. Fatty acid desaturation and the regulation of adiposity in *Caenorhabditis elegans*. *Genetics.* **176:** 865–875.
11. Clokey, G. V., and L. A. Jacobson. 1986. The autofluorescent lipofuscin granules in the intestinal-cells of *Caenorhabditis elegans* are secondary lysosomes. *Mech. Ageing Dev.* **35:** 79–94.
12. Hosokawa, H., N. Ishii, H. Ishida, K. Ichimori, H. Nakazawa, and K. Suzuki. 1994. Rapid accumulation of fluorescent material with aging in an oxygen-sensitive mutant Mev-1 of *Caenorhabditis elegans*. *Mech. Ageing Dev.* **74:** 161–170.
13. McKay, R. M., J. P. McKay, L. Avery, and J. M. Graff. 2003. C-elegans: a model for exploring the genetics of fat storage. *Dev. Cell.* **4:** 131–142.
14. Yang, F., B. W. Vought, J. S. Satterlee, A. K. Walker, Z. Y. J. Sun, J. L. Watts, R. DeBeaumont, R. M. Saito, S. G. Hyberts, S. Yang, et al. 2006. An ARC/Mediator subunit required for SREBP control of cholesterol and lipid homeostasis. *Nature.* **442:** 700–704.
15. Shibata, Y., R. Branicky, I. O. Landaverde, and S. Hekimi. 2003. Redox regulation of germline and vulval development in *Caenorhabditis elegans*. *Science.* **302:** 1779–1782.
16. Blaise, B. J., J. Giacomotto, M. N. Triba, P. Toulhoat, M. Piotto, L. Emsley, L. Segalat, M. E. Dumas, and B. Elena. 2009. Metabolic profiling strategy of *Caenorhabditis elegans* by whole-organism nuclear magnetic resonance. *J. Proteome Res.* **8:** 2542–2550.
17. Gunther, C. V., L. L. Georgi, and D. L. Riddle. 2000. A *Caenorhabditis elegans* type I TGF beta receptor can function in the absence of type II kinase to promote larval development. *Development.* **127:** 3337–3347.
18. Grant, B., and D. Hirsh. 1999. Receptor-mediated endocytosis in the *Caenorhabditis elegans* oocyte. *Mol. Biol. Cell.* **10:** 4311–4326.
19. Ntambi, J. M., M. Miyazaki, J. P. Stoehr, H. Lan, C. M. Kendziorski, B. S. Yandell, Y. Song, P. Cohen, J. M. Friedman, and A. D. Attie. 2002. Loss of stearoyl-CoA desaturase-1 function protects mice against adiposity. *Proc. Natl. Acad. Sci. USA.* **99:** 11482–11486.
20. Nakamura, M. T., and T. Y. Nara. 2004. Structure, function, and dietary regulation of Δ6, Δ5, and Δ9 desaturases. *Annu. Rev. Nutr.* **24:** 345–376.
21. Freudiger, C. W., W. Min, B. G. Saar, S. Lu, G. R. Holtom, C. W. He, J. C. Tsai, J. X. Kang, and X. S. Xie. 2008. Label-free biomedical imaging with high sensitivity by stimulated Raman scattering microscopy. *Science.* **322:** 1857–1861.
22. Hulbert, A. J., R. Pamplona, R. Buffenstein, and W. A. Buttemer. 2007. Life and death: metabolic rate, membrane composition, and life span of animals. *Physiol. Rev.* **87:** 1175–1213.
23. MacDonald, M. L. E., M. van Eck, R. B. Hildebrand, B. W. C. Wong, N. Bissada, P. Ruddle, A. Kontush, H. Hussein, M. A. Pouladi, M. J. Chapman, et al. 2009. Despite antiatherogenic metabolic characteristics, SCD1-deficient mice have increased inflammation and atherosclerosis. *Arterioscler. Thromb. Vasc. Biol.* **29:** 341–347.
24. Brown, J. M., S. Chung, J. K. Sawyer, C. Degirolamo, H. M. Alger, T. Nguyen, X. W. Zhu, M. N. Duong, A. L. Wibley, R. Shah, et al. 2008. Inhibition of stearoyl-coenzyme A desaturase 1 dissociates insulin resistance and obesity from atherosclerosis. *Circulation.* **118:** 1467–1475.
25. Ogretmen, B., and Y. A. Hannun. 2004. Biologically active sphingolipids in cancer pathogenesis and treatment. *Nat. Rev. Cancer.* **4:** 604–616.
26. Cao, H., K. Gerhold, J. R. Mayers, M. M. Wiest, S. M. Watkins, and G. S. Hotamisligil. 2008. Identification of a lipokine, a lipid hormone linking adipose tissue to systemic metabolism. *Cell.* **134:** 933–944.
27. Kopelman, P. G. 2000. Obesity as a medical problem. *Nature.* **404:** 635–643.
28. Dupuy, D., N. Bertin, C. A. Hidalgo, K. Venkatesan, D. Tu, D. Lee, J. Rosenberg, N. Svrzikapa, A. Blanc, A. Carnec, et al. 2007. Genome-scale analysis of in vivo spatiotemporal promoter activity in *Caenorhabditis elegans*. *Nat. Biotechnol.* **25:** 663–668.
29. Chung, K., M. M. Crane, and H. Lu. 2008. Automated on-chip rapid microscopy, phenotyping and sorting of *C. elegans*. *Nat. Methods.* **5:** 637–643.
30. Evans, C. L., E. O. Potma, M. Puoris'haag, D. Cote, C. P. Lin, and X. S. Xie. 2005. Chemical imaging of tissue in vivo with video-rate coherent anti-Stokes Raman scattering microscopy. *Proc. Natl. Acad. Sci. USA.* **102:** 16807–16812.
31. Huff, T. B., and J. X. Cheng. 2007. In vivo coherent anti-Stokes Raman scattering imaging of sciatic nerve tissue. *J. Microsc.* **225:** 175–182.
32. Zhu, J., B. Lee, K. K. Buhman, and J. X. Cheng. 2009. A dynamic cytoplasmic triacylglycerol pool in enterocytes revealed by ex vivo and in vivo coherent anti-Stokes Raman scattering imaging. *J. Lipid Res.* **50:** 1080–1089.

ERRATA

The authors of "Label-free quantitative analysis of lipid metabolism in living *Caenorhabditis elegans*" (*J. Lipid Res.* 51: 672–677) have advised the *Journal* that the figure legend for Figure 2 of their manuscript is incorrect. It should read as follows:

Fig. 2. Expression levels of lipid species in the wild type and mutant *C. elegans*. A: CARS imaging of lipid (red) and TPEF imaging of autofluorescent lipid species (blue) of adult N2 wild-type and mutant *C. elegans*. Images are presented as three-dimensional projections of 36 frames taken along the vertical axis at 1 μm intervals. Expression levels of neutral lipid droplets (B) and autofluorescent lipid droplets (C) as a function of wild-type and mutant worms. Expression levels are normalized to 1 for the wild type and comparatively for mutants. Error bars represent distribution across six adult wild-type or mutant *C. elegans*. D: Biochemical measurements of cholesterol level and superoxide dismutase (SOD) activity. Expression levels are normalized to 1 for the wild type and comparatively for mutant *C. elegans*. Error bars represent distribution across three repeated experiments.

The incorrect figure legend initially appeared online but has since been corrected.

DOI 10.1194/jlr.D000638ERR

The authors of "Production and characterization of monoclonal anti-sphingosine-1-phosphate antibodies" (*J. Lipid Res.* 50: 2245–2257) have advised the *Journal* that the name of an oligo stated in the Materials and Methods section of their manuscript is incorrect. The mouse immunoglobulin kappa chain variable region (VL) was amplified by PCR using **VK20**, not MKV20.

This incorrect oligo name initially appeared online but has since been corrected.

DOI 10.1194/jlr.M900048ERR